Highlights

Optimal Design of Tuned Liquid Column Damper Inerter for vibration control

Di Matteo A., Masnata C., Adam C., Pirrotta A.

- Optimal design of Tuned Liquid Column Damper Inerter for single degree of freedom structures is studied;
- A straightforward numerical approach is developed for its optimization;
- An analytical solution for the optimal design of TLCDI parameters is derived;
- Analyses are performed using random base excitations and real earthquake records.

Optimal Design of Tuned Liquid Column Damper Inerter for vibration control

Di Matteo A.[a], Masnata C.[a,*], Adam C.[b], Pirrotta A.[a]

[a] *Department of Engineering, University of Palermo, viale delle Scienze, 90128 Palermo, Italy.*
[b] *Unit of Applied Mechanics, University of Innsbruck, Technikerstr. 13, Innsbruck, Austria*

Abstract

In this paper, the use of a novel passive control device defined as Tuned Liquid Column Damper Inerter (TLCDI) is studied to control the seismic response of structural systems. The TLCDI, recently introduced as an enhanced version of the conventional Tuned Liquid Column Damper, may achieve improved seismic performances by exploiting the mass amplification effect of the so-called inerter device. For this purpose, an optimization procedure for the design of the TLCDI based on a statistical linearization technique and the minimization of the structural displacement variance is proposed. Notably, by assuming a white noise base excitation and considering some additional approximations, pertinent closed-form expressions for the optimal TLCDI parameters are provided. The reliability of the proposed analytical solutions is proved by a comparison with numerical results obtained by a more computationally demanding iterative optimization technique on the original damped system. Finally, the efficiency of the control performance of TLCDI-controlled structures is examined using real recorded seismic signals as external excitation.

Keywords: Tuned Liquid Column Damper, Inerter, Optimal design, Statistical Linearization Technique

1. Introduction

In the field of passive vibration control devices, the use of mechanical dampers has nowadays become a common strategy to mitigate vibrations of structures subjected to dynamic loads. In this context, Tuned Mass Dampers (TMDs) [1, 2], Tuned Liquid Dampers (TLDs) [3–5] and Tuned Liquid Column Dampers (TLCDs) [6, 7] are among the most widely used damping devices for reducing structural vibrations caused by wind or earthquakes. They have been already installed on the top of many tall buildings and proved to be efficient in successfully protecting these structures from real dynamic excitation.

However, these devices may require large masses to be effective. Consequently, the idea to combine these dampers with mass amplifying mechanisms, such as inerter-based devices, has gradually became the current favoured trend

*Corresponding author
Email address: chiara.masnata@unipa.it (Masnata C.)

for structural vibration control. The inerter, firstly introduced by M. Smith [8, 9], is a two terminal mechanical device capable to generate a resisting force proportional to the accelerations of its extremities with a constant referred to as inertance, measured in mass units. Technologically, inerter prototypes, with inertance values hundreds of times larger than the device physical mass, have been experimentally tested considering mechanisms transforming the translational motion of the device ends into rotational motion (i.e. rack and pinion, ball-screw and fluid inerters) [10–13]. Notably, the inclusion of the inerter virtually increases the effect of the mass of the secondary system to which it is connected [14]. In this regard, the inerter has been firstly integrated in the classical TMD to constitute a device known in literature as Tuned Mass Damper Inerter (TMDI) [15]. In this way, the inerter is able of generating a sort of mass amplification effect, making the TMDI behaving like a TMD with a larger mass, to achieve enhanced performance compared to the classical TMD.

In [15] it has been demonstrated that the TMDI outperforms the TMD in controlling structural vibrations and proposed analytical formulae of the optimal TMDI parameters to design the device. Many variants of inerter-based configurations have been developed in recent years. The installation of the TMDI has been considered also for base isolated structures with the aim of reducing the displacements of the base isolation system during severe earthquakes [16, 17]. Moreover, a nontraditional version of the TMDI, referred to as New TMDI, obtained varying the damper position, has been introduced in [18] as an alternative and more practical solution to reduce vibrations in base isolated structures.

Clearly, following the trend related to the development of the TMDI, some liquid-based devices have been proposed in combination with the inerter as promising passive control strategies [19–21]. Liquid-based dampers, such as the TLDs [3] and TLCDs [6], are containers filled with liquid (usually water) rigidly fixed to the structure to be controlled and their capacity to absorb and dissipate vibration energy depends essentially on the motion of the liquid inside. Compared to the several types of TMDs, liquid-based dampers show some convenient characteristics such as low cost, easy implementation, lack of required maintenance, the possibility to use the liquid for both water supply and fire-fighting purposes. In this regards, by combining the advantage of TLD and the inerter, in [19] a novel device, the Tuned Liquid Inerter system (TLIS) has been proposed. In this study, they derived a closed form solution of the TLIS optimal parameters for an undamped single degree of freedom (SDOF) system. They concluded that the TLIs can achieve the same or even higher mitigation effects with a smaller quantity of liquid mass compared to the classical TLD.

Further, in [20] it has been showed that significant improvement, over the classical TLCD, can be achieved by integrating an inerter in the TLCD itself. The TLCDI dissipates the structural vibrations by means of a combined action which involves the vertical motion of the liquid inside a U-shape tank and the horizontal motion of the container. Indeed, unlike the classical TLCD, the TLCDI is supposed to be able to translate through a sliding support and it is connected to the structure by a linear spring and a damper and to the ground by an inerter. In [21], benefits due to the installation of a TLCDI as link between high-rise adjacent buildings to control their seismic response have been investigated.

Clearly, the optimal design of the TLCDI plays a key role to obtain the

best mitigation effect of the structural response. However, note that in all the previous studies the optimal TLCDI parameters have been derived for TLCDI controlled structures only by means of numerical procedures based on the minimization of different objective functions (see [20] and references therein). Therefore, these procedures may be computationally demanding in a design phase and may lead to parameters not easily applicable in real design processes [20].

On this base, the present work focuses on providing analytical closed-form solutions for determining, in a straightforward way, the TLCDI optimal design parameters for a SDOF structure subjected to a base excitation. In this regard, the nonlinear equations of motion are established and TLCDI optimal parameters are evaluated by taking into account a statistical linearization technique. Specifically, the proposed optimization procedure is based on the minimization of the variance of the structural response, which is found in closed-form by assuming some reasonable hypotheses. Notably, the obtained closed-form expression leads to very accurate results, without requiring any computational effort as in the case of classical numerical procedures. In this manner, the effectiveness of the optimized TLCDI on the seismic response of structures is investigated. In particular, the control performance of TLCDI controlled structures is discussed for both white noise excitation, broad-band excitation, as well as considering real earthquake records. Numerical analyses have confirmed the validity of the proposed optimization procedure, even for real seismic records, indicating that coupling the inerter with a TLCD device significantly reduces the structural responses of the uncontrolled structure compared to the traditional TLCD.

2. Problem formulation

Consider the case of a SDOF system (main structure) equipped with a TLCDI device, as shown in Fig. 1, under a base excitation. The TLCDI, as shown

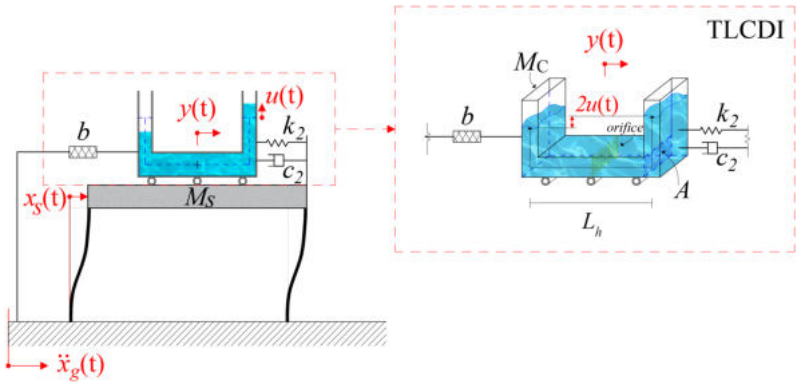

Figure 1: SDOF structure equipped with a TLCDI.

in Fig. 1 comprises a U-shape tank characterized by a cross sectional area A, with dimensions L_v and L_h for the vertical and horizontal liquid length, respectively; thus, $L = L_h + 2L_h$ is the total length of the liquid inside the TLCDI. The mass of the container is M_c, while the liquid mass is $m_l = \rho AL$ being ρ the density of the liquid. The TLCDI is connected to the main structure by a spring

and a damper with stiffness and damping coefficient k_2 and c_2, respectively, and to the ground by an inerter element with inertance b. The vertical motion of the liquid in the U-shape tube is denoted as $u(t)$, while the horizontal motion of the container relative to the primary structure is $y(t)$. As far as the SDOF structure is concerned, M_s indicates the mass, K_s and C_s are the stiffness and damping parameters, respectively, and $x_s(t)$ is the displacement of the main system relative to the ground. The response of this TLCDI-equipped SDOF structure subjected to a horizontal ground acceleration $\ddot{x}_g(t)$, is governed by the following equations [20]

$$
\begin{aligned}
&M_s\ddot{x}_s(t) + C_s\dot{x}_s(t) + K_s x_s(t) - c_2\dot{y}(t) - k_2 y(t) = -M_s\ddot{x}_g(t) \\
&(\rho AL + M_c + b)\,\ddot{y}(t) + (\rho AL + M_c + b)\,\ddot{x}_s(t) + \rho AL_h\ddot{u}(t) + c_2\dot{y}(t) + k_2 y(t) = \\
&= -(\rho AL + M_c)\,\ddot{x}_g(t) \\
&\rho AL_h\ddot{x}_s(t) + \rho AL_h\ddot{y}(t) + \rho AL\ddot{u}(t) + \tfrac{\rho A}{2}\xi|\dot{u}(t)|\dot{u}(t) + 2\rho A g u(t) = -\rho AL_h\ddot{x}_g(t)
\end{aligned}
\tag{1}
$$

where g is the gravity acceleration, a dot over a variable stands for derivation with respect to time t, and ξ is the so-called head loss coefficient, introduced to represent the hydrodinamic head losses that arise during the motion of the liquid inside the vessel [22–24]. Further, dividing Eq. 1 by M_s, and by ρAL the last two equations, yields

$$
\begin{aligned}
&(1 + \mu_t + \beta)\,\ddot{x}_s(t) + (\mu_t + \beta)\,\ddot{y}(t) + \alpha\mu_l\ddot{u}(t) + 2\omega_s\zeta_s\dot{x}_s(t) + {\omega_s}^2 x_s(t) = \\
&= -(1 + \mu_t)\,\ddot{x}_g(t) \\
&(\mu_t + \beta)\,\ddot{x}_s(t) + (\mu_t + \beta)\,\ddot{y}(t) + \alpha\mu_l\ddot{u}(t) + 2\mu_t\omega_2\zeta_2\dot{y}(t) + \mu_t{\omega_2}^2 y(t) = -\mu_t\ddot{x}_g(t) \\
&\alpha\ddot{x}_s(t) + \alpha\ddot{y}(t) + \ddot{u}(t) + \tfrac{1}{2L}\xi|\dot{u}(t)|\dot{u}(t) + {\omega_l}^2 u(t) = -\alpha\ddot{x}_g(t)
\end{aligned}
\tag{2}
$$

where $\omega_s = \sqrt{K_s/M_s}$ and $\zeta_s = C_s/(2\omega_s M_s)$ are the natural frequency and damping ratio of the main SDOF structure, while $\alpha = L_h/L$ is the length ratio and $\beta = b/M_s$ the inertance ratio. Further, $\mu_t = \mu_l + \delta$ denotes the total mass ratio where $\mu_l = \rho AL/M_s$ and $\delta = M_c/M_s$, are the liquid and the container mass ratio, respectively.

In addition, $\omega_2 = \sqrt{k_2/(\mu_t M_s)}$ and $\zeta_2 = c_2/(2\omega_2\mu_t M_s)$ are the natural frequency and damping ratio of the liquid container, and $\omega_l = \sqrt{2g/L}$ is the natural frequency of oscillation of the liquid inside the TLCDI. Note that Eqs. 2 represent a set of three differential equations, with the second comprising a nonlinear term, generally used to model head losses caused by the presence of an orifice inside the TLCDI and viscous interaction between the liquid and rigid container wall [25–27]. Since the damping term in Eq. 2 is nonlinear, even assuming that the main structure behaves linearly, the whole system experiences inherent nonlinear properties. Consequently, some issues may arise for the optimal design of the damper device aiming at reaching the maximum reduction of the displacement demand of the SDOF system. For this reason, an equivalent linearization procedure, which facilitates the optimal design process, is considered here.

2.1. Statistical linearization technique

The nonlinear equations of motion Eqs. 2 can be linearized by adopting techniques such as the Statistical Linearization Technique (SLT). In this regard, suppose that the main SDOF system equipped with a TLCDI is driven by a random excitation modeled as a zero mean Gaussian white noise process. It follows that liquid and system displacements and their derivatives are stochastic processes too (denoted by capital letters, as customary) [27]. Thus, taking full advantage of the powerful tool of the SLT, the original nonlinear system Eqs. 2 can be replaced by a linear equivalent one as

$$\begin{aligned}
&(1+\mu_t+\beta)\,\ddot{X}_s(t)+(\mu_t+\beta)\,\ddot{Y}(t)+\alpha\mu_l\ddot{U}(t)+2\omega_s\zeta_s\dot{X}_s(t)+{\omega_s}^2X_s(t)=\\
&=-(1+\mu_t)\,\ddot{X}_g(t)\\
&(\mu_t+\beta)\,\ddot{X}_s(t)+(\mu_t+\beta)\,\ddot{Y}(t)+\alpha\mu_l\ddot{U}(t)+2\mu_t\omega_2\zeta_2\dot{Y}(t)+\mu_t{\omega_2}^2Y(t)=-\mu_t\ddot{X}_g(t)\\
&\alpha\ddot{X}_s(t)+\alpha\ddot{Y}(t)+\ddot{U}(t)+2\omega_l\zeta_l\dot{U}(t)+{\omega_l}^2U(t)=-\alpha\ddot{X}_g(t)
\end{aligned} \tag{3}$$

which is now simply a set of three linear differential equations. Specifically, the term $\frac{1}{2L}\xi|\dot{U}(t)|\dot{U}(t)$ has been replaced by $2\omega_l\zeta_l\dot{U}(t)$ and the equivalent damping ratio ζ_l has been introduced. The error between the nonlinear TLCDI-SDOF system and its equivalent linear is

$$\epsilon=\tfrac{1}{2L}\xi|\dot{U}(t)|\dot{U}(t)-2\omega_l\zeta_l\dot{U}(t) \tag{4}$$

Therefore, the term ζ_l is obtained minimizing the mean square of the error with respect to ζ_l [28]. Specifically, following the analysis in [25, 29, 30], the expression for the equivalent damping ratio becomes

$$\zeta_l=\tfrac{\xi}{2L\omega_l}\sqrt{\tfrac{2}{\pi}}\sigma_{\dot{U}} \tag{5}$$

where $\sigma_{\dot{U}}$ is the standard deviation of the velocity of the liquid inside in the TLCDI defined as in Appendix A.

3. Optimization procedure

Once the equations of motion are stated, the determination of the optimal TLCDI design parameters can be pursued. As it can be seen in Eq. 3, in general there are seven main TLCDI parameters governing the response of the system, that is: the inertance ratio β, the mass ratios μ_l and δ, the natural frequency ω_2, the damping ratio ζ_2 of the container, the natural frequency ω_l, the equivalent damping ratio ζ_l of the liquid and the length ratio α. Clearly, best control performances can be obtained only appropriately chosing the aforementioned parameters. However, some of these variables are often determined a priori due to structural constraints, such as μ_l, β, δ and α.

Therefore, only the design parameters ζ_2, ζ_l, ω_l and ω_2 (or equivalently the so-called frequency ratios $\nu_l=\omega_l/\omega_s$ and $\nu_2=\omega_2/\omega_s$), are required to be appropriately chosen through an optimization procedure.

As usually done in the relevant literature for TLCDI-based control strategies, these parameters can be sought by minimizing a specific quantity representative of the dynamic response of the structural system, such as the response in terms of displacement or acceleration variance of the considered system. In this regard, the structural displacement variance of the main SDOF structure is here employed as the objective of the optimization procedure. Specifically, the response variance in terms of displacement can be expressed as

$$\sigma_{X_s}^2 = \int_0^\infty |H_{X_s}(\omega)|^2 G_0 \, d\omega \tag{6}$$

in which G_0 is the one-sided Power Spectral Density (PSD) of the white noise input and $H_{X_s}(\omega)$ is the displacement transfer function of the main structure in the equivalent linear system described by Eqs. 3, defined as in Appendix A.

However, in this case, the mean-square responses need to be calculated numerically by means of algorithms which might result cumbersome and time consuming in design phases [19–21]. Moreover, as far as the optimization of the equivalent damping ratio ζ_l is concerned, an iterative procedure has to be pursued since $\sigma_{\dot{U}}$ is unknown and implicitly depends on ζ_l, thus, the use of Eq. 5 for design purposes is not straightforward [20, 25, 30, 31] (see Appendix A for details).

Therefore, in order to provide a tool to promptly compute the optimal TLCDI parameters, a direct analytical approach is proposed in the following section.

3.1. Approximate evaluation of the response variance

In order to determine the optimal design parameters of the TLCDI in a straightforward manner, a closed-form solution in terms of steady state response statistics is proposed. In this regard, Eqs. 3 are recast in compact matrix form as

$$\tilde{\mathbf{M}}\ddot{\mathbf{Z}} + \tilde{\mathbf{C}}\dot{\mathbf{Z}} + \tilde{\mathbf{K}}\mathbf{Z} = -\tilde{\mathbf{M}}\tilde{\mathbf{r}}\ddot{x}_g \tag{7}$$

where $\mathbf{Z} = \begin{bmatrix} X_s(t) & Y(t) & U(t) \end{bmatrix}^T$ is the vector collecting the displacement of the degrees of freedom, $\tilde{\mathbf{r}} = \begin{bmatrix} 1 & \frac{\beta}{\alpha^2\mu_l - \beta - \mu_t} & \frac{\beta}{\alpha^2\mu_l - \beta - \mu_t} \end{bmatrix}^T$ is the location vector and the transpose operation is denoted with the apex T.

$\tilde{\mathbf{M}}$, $\tilde{\mathbf{C}}$, and $\tilde{\mathbf{K}}$ are the mass matrix, the damping matrix and the stiffness matrix, respectively, particularized as

$$\tilde{\mathbf{M}} = \begin{bmatrix} 1+\mu_t+\beta & \mu_t+\beta & \alpha\mu_l \\ \mu_t+\beta & \mu_t+\beta & \alpha\mu_l \\ \alpha & \alpha & 1 \end{bmatrix}$$

$$\tilde{\mathbf{C}} = \begin{bmatrix} 2\zeta_s\omega_s & 0 & 0 \\ 0 & 2\zeta_2\omega_2\mu_t & 0 \\ 0 & 0 & 2\zeta_l\omega_l \end{bmatrix} \tag{8}$$

$$\tilde{\mathbf{K}} = \begin{bmatrix} \omega_s^2 & 0 & 0 \\ 0 & \mu_t\omega_2^2 & 0 \\ 0 & 0 & \omega_l^2 \end{bmatrix}$$

Since the input is modeled as a zero-mean stationary Gaussian white noise process, the corresponding Lyapunov equation of the evolution of the covariance matrix [25] can be written as

$$\dot{\Sigma}_{\mathbf{Q}}(t) = \mathbf{D_S}\Sigma_{\mathbf{Q}}(t) + \Sigma_{\mathbf{Q}}(t)\,\mathbf{D_s^T} + \mathbf{G_S}\mathbf{G_S^T}\pi G_0 \tag{9}$$

where $\mathbf{Q} = \begin{bmatrix} \mathbf{Z} & \dot{\mathbf{Z}} \end{bmatrix}^T$ is the vector of the state variables, $\Sigma_{\mathbf{Q}}(t)$ represents the covariance matrix given as

$$\Sigma_{\mathbf{Q}} = \begin{bmatrix} \sigma^2_{X_s} & \sigma^2_{X_sY} & \sigma^2_{X_sU} & \sigma^2_{X_s\dot{X}_s} & \sigma^2_{X_s\dot{Y}} & \sigma^2_{X_s\dot{U}} \\ & \sigma^2_{Y} & \sigma^2_{YU} & \sigma^2_{Y\dot{X}_s} & \sigma^2_{Y\dot{Y}} & \sigma^2_{Y\dot{U}} \\ & & \sigma^2_{U} & \sigma^2_{U\dot{X}_s} & \sigma^2_{U\dot{Y}} & \sigma^2_{U\dot{U}} \\ & & & \sigma^2_{\dot{X}_s} & \sigma^2_{\dot{X}_s\dot{Y}} & \sigma^2_{\dot{X}_s\dot{U}} \\ sym & & & & \sigma^2_{\dot{Y}^2} & \sigma^2_{\dot{Y}\dot{U}} \\ & & & & & \sigma^2_{\dot{U}} \end{bmatrix} \tag{10}$$

while $\mathbf{D_S}$ and $\mathbf{G_S}$ are given as [32]

$$\mathbf{D_S} = \begin{bmatrix} \mathbf{0} & \mathbf{I_3} \\ -\tilde{\mathbf{M}}^{-1}\tilde{\mathbf{K}} & -\tilde{\mathbf{M}}^{-1}\tilde{\mathbf{C}} \end{bmatrix}, \quad \mathbf{G_S} = \begin{bmatrix} \mathbf{0} \\ \tilde{\mathbf{r}} \end{bmatrix} \tag{11}$$

with $\mathbf{I_3}$ a 3×3 identity matrix.

Solution of Eq. 9 gives the evolution of all the response statistics of the system in Eqs. 3. However, since only the steady-state variance must be computed, $\dot{\Sigma}_{\mathbf{Q}}(t)$ can be equated to zero.

Further, with the aim of directly determining the optimal parameters, the analytical form of the structural displacement variance $\sigma^2_{X_s}$ is required and some additional approximations need to be introduced. Specifically, the approximate behavior of an undamped SDOF structure can be assumed, as customary in many optimization procedures for passive vibration control systems [15, 19]. Next, considering that the damping effect of the liquid is typically small [33], in this phase the presence of the damping term is neglected [19]. Notably, in the following it will be shown how ζ_l can be estimated as a function of the optimal design parameters obtained hereinafter.

Overall, on this base, only the design parameters ζ_2, ν_l and ν_2 are required and introducing the aforementioned assumptions into Eq. 9, after some algebra, the system displacement variance is derived in an analytical form as

$$\sigma^2_{X_s} = \frac{\pi G_0}{4 z_{X_s} \omega_s^3} \tag{12}$$

in which $z_{X_s} = \frac{N_Z}{D_Z}$ with

$$N_Z = \zeta_2 \mu_t \nu_2 \nu_l{}^2 \left[\alpha^2 \mu_l + (\beta + \mu_t)\left(-1 + \nu_l{}^2\right)\right]^2 \tag{13}$$

$$
\begin{aligned}
D_Z =& {\nu_l}^2 \left[\alpha^2\mu_l + \beta(-1+{\nu_l}^2) + \mu_t(-1+{\nu_l}^2)\right]^2 + {\nu_2}^2\mu_t{\nu_l}^2\left[-3\alpha^4{\mu_l}^2 + \alpha^4{\mu_l}^2{\mu_t}^2 + \right. \\
&+ 4\alpha^4{\zeta_2}^2{\mu_l}^2\mu_t(3-\beta+\mu_t) - 2\alpha^2\mu_l\left(-1-2\beta^2{\zeta_2}^2\mu_t + \beta(-2+4{\zeta_2}^2\mu_t+{\mu_t}^2) + \right. \\
&\left.+\mu_t(-3+{\mu_t}^2+2{\zeta_2}^2(3+2\mu_t(3+\mu_t)))\right) + 2\alpha^2\mu_l\left(-1+\beta(-2+{\mu_t}^2)+\mu_t(-3+\right. \\
&\left.+{\mu_t}^2+4{\zeta_2}^2(1+\mu_t)(2+\mu_t))\right){\nu_l}^2 + (1+\mu_t)(\beta^2(-1+\mu_t)+\mu_t(1+\mu_t)(-2+\mu_t+ \\
&+4{\zeta_2}^2(1+\mu_t)) + 2\beta\left(-1+\mu_t(-1+\mu_t+2{\zeta_2}^2(1+\mu_t))\right))\left(-1+{\nu_l}^2\right)^2\Big] + \\
&+ {\nu_2}^4\left[\alpha^6{\mu_l}^3{\mu_t}^2 - 2\alpha^4{\mu_l}^2{\mu_t}^2(\beta+\mu_t) + \alpha^2\mu_l{\mu_t}^2(\beta+\mu_t)^2 - 2\alpha^2\mu_l{\mu_t}^2(1+\mu_t)\,(2+\right. \\
&\left.+\beta(3+\mu_t)+\mu_t(4+\mu_t))\,{\nu_l}^2 + \alpha^4{\mu_l}^2{\mu_t}^2\,(6+\mu_t(6+\mu_t))\,{\nu_l}^2 + \alpha^2\mu_l{\mu_t}^2(1+\mu_t)\,(5+\right. \\
&\left.+7\mu_t+2{\mu_t}^2+2\beta(2+\mu_t))\,{\nu_l}^4 + (1+\beta+\mu_t)^2(\mu_t+{\mu_t}^2)^2{\nu_l}^2(-1+{\nu_l}^2)^2\right]
\end{aligned}
\tag{14}
$$

Taking into account Eq. 12, one may directly look for the minimum of the smooth function

$$
\phi\left(\zeta_2, \nu_l, \nu_2\right) = \frac{1}{z_{X_s}} \tag{15}
$$

which is independent of G_0 and of the natural frequency of the main system ω_s. In this regard, a sample of the function $z_{X_s}\left(\zeta_2, \nu_l, \nu_2\right)$ is shown in Fig. 2 for $\nu_l = 0.4$.

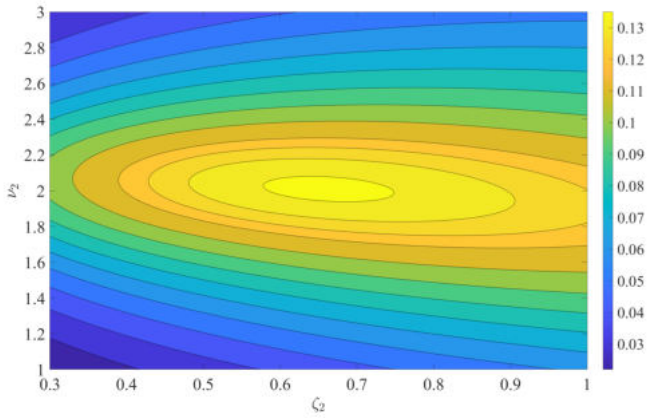

Figure 2: Contour plot of $z_{X_s}\left(\zeta_2, \nu_l, \nu_2\right)$ (for α=0.9, $\delta = 0.01$, $\beta = 0.3$, $\nu_l = 0.4$, $\mu_l = 0.04$).

In general, an analytical expression for the minimum of $\phi\left(\zeta_2, \nu_l, \nu_2\right)$ could be obtained, solving the nonlinear system of algebraic equations

$$
\frac{\partial\phi\left(\zeta_2, \nu_l, \nu_2\right)}{\partial\zeta_2} = 0 \tag{16a}
$$

$$
\frac{\partial\phi\left(\zeta_2, \nu_l, \nu_2\right)}{\partial\nu_2} = 0 \tag{16b}
$$

$$
\frac{\partial\phi\left(\zeta_2, \nu_l, \nu_2\right)}{\partial\nu_l} = 0 \tag{16c}
$$

However, this procedure is often unfeasible, thus the minimum of $\phi\left(\zeta_2, \nu_l, \nu_2\right)$ in Eq. 15 can be more easily found through numerical minimization procedure, such as those already implemented in many software packages (see for instance FindMinimum in Mathematica or fminsearch in MATLAB environment). In this way, Eq. 15 provides the optimal design parameter values ζ_2, ν_l and ν_2.

3.2. Analytical expression of the optimal design parameters

Aiming at further reducing the computational complexity in a desgin phase of the TLCDI, an analytical expression of the optimal design parameters can be achieved considering some additional assumptions. As it can be seen in Eqs. 13-14, the function $\sigma^2_{\bar{X}_s}$ in Eq. 12 depends on the mass ratios μ_l and μ_t. Since generally $\mu_l < 5\%$ and $\mu_t < 1\%$, solutions of Eq. 16 can be approximated by assuming that the third and higher powers of μ_l, μ_t and their products can be neglected [3, 34]. In particular, under these assumptions, Eqs. 16a- 16b can be directly solved, and the expressions of $\tilde{\nu}_{2,opt}(\nu_l)$ and $\tilde{\zeta}_{2,opt}(\nu_l)$ can be expressed as functions of ν_l as

$$\tilde{\nu}_{2,opt}(\nu_l) = \sqrt{A/B} \tag{17}$$

$$\tilde{\zeta}_{2,opt}(\nu_l) = \sqrt{C/D} \tag{18}$$

with

$$\begin{aligned} A =& \nu_l{}^2 \left[-(\beta^2(-1+\mu_t{}^2)(-1+\nu_l{}^2)^2) + 2\beta(-1+\nu_l{}^2)(2\alpha^2\mu_l + (1+2\mu_t)(-1+\nu_l{}^2)) + \right. \\ & \left. + (\alpha^2\mu_l + \mu_t(-1+\nu_l{}^2))(3\alpha^2\mu_l + (2+3\mu_t)(-1+\nu_l{}^2))\right] \end{aligned} \tag{19}$$

$$B = -2\mu_t \left[(1+\beta)(1+\beta+2(2+\beta)\mu_t)\nu_l{}^2\left(-1+\nu_l{}^2\right)^2 + \alpha^2\mu_l\left(\beta^2 - 2(2+3\beta)\nu_l{}^2 + (5+4\beta)\nu_l{}^4\right)\right] \tag{20}$$

$$\begin{aligned} C =& -\left[\beta^2(4+3\beta) + \beta(8+\beta(21+8\beta))\mu_t + (4+3\beta(11+2\beta(6+\beta)))\mu_t{}^2\right]\nu_l{}^2\left(-1+\nu_l{}^2\right)^3 + \\ & + \alpha^4\mu_l^2\left[-12\beta^2 + (4+\beta)(1+8\beta)\nu_l{}^2 - (8+25\beta)\nu_l{}^4\right] - \alpha^2\mu_l\left(-1+\nu_l{}^2\right)\left[4\beta^2(\beta+3\mu_t) + \right. \\ & \left. -(8\mu_t + \beta(8+66\mu_t+\beta(21+40\mu_t)))\nu_l{}^2 + (12\mu_t + \beta(12+58\mu_t+\beta(13+32\mu_t)))\nu_l{}^4\right] \end{aligned} \tag{21}$$

$$\begin{aligned} D =& -8\mu_t\nu_l{}^2\left(-1+\nu_l{}^2\right)\left[\alpha^2\beta^3\mu_l + \beta^2(1+2\mu_t)\left(-1+\nu_l{}^2\right)^2 + (2+9\mu_t)\left(-1+\nu_l{}^2\right)^2 + \right. \\ & \left. + \alpha^2\mu_l\left(-9+11\nu_l{}^2\right) + \beta\left((3+10\mu_t)\left(-1+\nu_l{}^2\right)^2 + \alpha^2\mu_l\left(-10+7\nu_l{}^2\right)\right)\right] \end{aligned} \tag{22}$$

In Figs. 3a- 3b the approximated solutions of the optimal parameters $\tilde{\nu}_{2,opt}(\nu_l)$ and $\tilde{\zeta}_{2,opt}(\nu_l)$ in Eqs. 17- 18, are compared with those obtained numerically

solving Eqs. 16a- 16b, respectively for several values of μ_l. As it emerges from Fig. 3, it can be argued that the approximated solutions of the optimal parameters $\tilde{\nu}_{2,opt}(\nu_l)$ and $\tilde{\zeta}_{2,opt}(\nu_l)$ in Eqs. 17- 18 closely agree with the numerical solution of Eqs. 16.

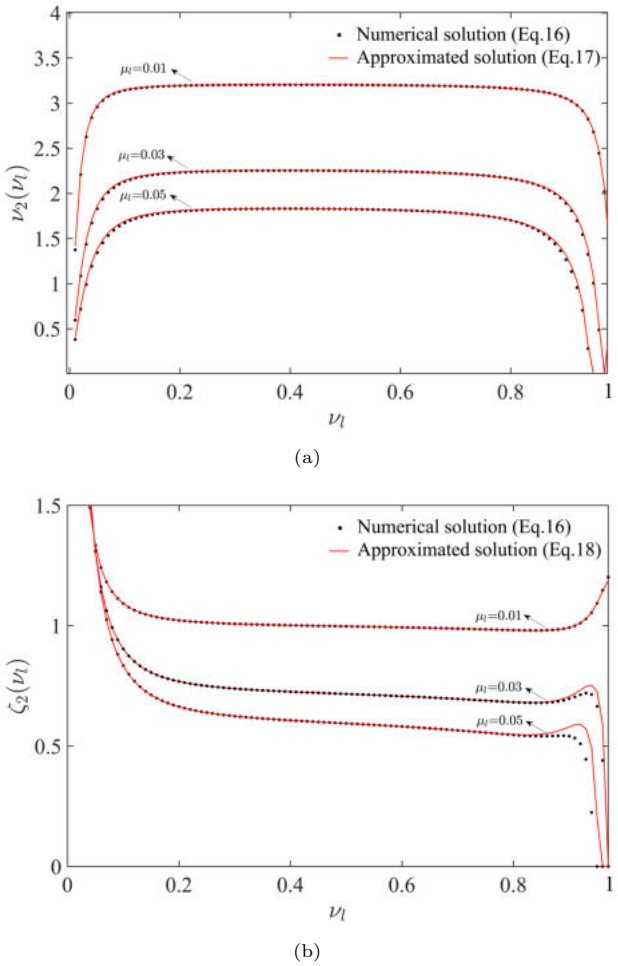

Figure 3: Approximated solutions versus numerical solutions of Eq. 16c for different values of μ_l (for α=0.9, $\delta = 0.01$, $\beta = 0.3$): (a) $\tilde{\nu}_{2,opt}(\nu_l)$; (b) $\tilde{\zeta}_{2,opt}(\nu_l)$.

Moreover, Fig. 3 shows that the optimal parameters $\tilde{\nu}_{2,opt}(\nu_l)$ and $\tilde{\zeta}_{2,opt}(\nu_l)$ decrease for increasing values of μ_l with an almost steady trend for $0.2 < \nu_l < 0.8$, suggesting that $\tilde{\nu}_{2,opt}(\nu_l)$ and $\tilde{\zeta}_{2,opt}(\nu_l)$ are almost independent of values of ν_l in the range of practical interest.

Finally, optimal values of $\nu_{l,opt}$ which minimize the smoth function $\phi(\zeta_2, \nu_l, \nu_2)$ can be found by solving Eq. 16c. In this regard, in Fig. 4, the trend of $\partial\phi(\zeta_2, \nu_l, \nu_2)/\partial\nu_l$ is depicted. As it can be seen, this derivative is zero for the optimal value of $\nu_{l,opt} = 0.4331$. Nonetheless, since a wide range of values of ν_l (0.2¡ν_l¡0.6) lead to values of $\partial\phi(\zeta_2, \nu_l, \nu_2)/\partial\nu_l$ close to zero, it can be concluded that small variations of ν_l in this range may just slightly affect the achievement of the minimum.

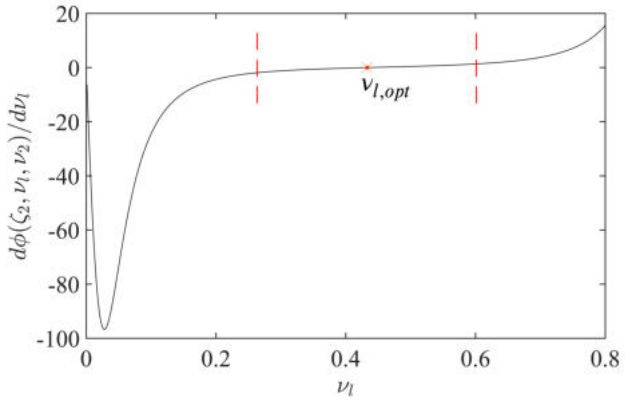

Figure 4: $\partial\phi\,(\zeta_2, \nu_l, \nu_2)/\partial\nu_l$ (for $\alpha = 0.9$, $\mu_l = 0.04$, $\beta = 0.3$, $\zeta_s = 0.01$).

Clearly, the expressions of $\tilde{\nu}_{2,opt}(\nu_l)$ and $\tilde{\zeta}_{2,opt}(\nu_l)$ in Eqs. 17- 18 can be substituted in Eq. 16c to obtain a closed form solution of $\nu_{l,opt}$. Since this approach leads to a rather unwieldy expression of $\nu_{l,opt}$, this formula is not reported here for the sake of brevity.

However, in order to provide optimal values of $\nu_{l,opt}$, which can be directly used in a desgin phase, this procedure can be also used to create immediately useful design charts for several values of μ_l, β α, and δ. Specifically, the charts depicted in Fig. .14 show optimal values in terms of $\nu_{l,opt}$ for different values of β and μ_l. For instance, suppose that a length ratio $\alpha = 0.8$ is chosen, the inertance ratio β is equal to 0.3, the mass ratios given by structural constraints are μ_l= 3% and $\delta = 1\%$, thus identifying the point A in Fig. 5b. This design chart directly provides the optimal parameters $\nu_{l,opt}$= 0.4345. Additional desgin charts are provided in Appendix B for other values of β and δ.

Clearly, once the value of $\nu_{l,opt}$ is determined, Eq. 17 and Eq. 18 can be used for a straightforward determination of the optimal TLCDI design parameters $\tilde{\nu}_{2,opt}(\nu_l)$ and $\tilde{\zeta}_{2,opt}(\nu_l)$. Finally, as far as the determination of the optimal head loss coefficient is concerned, an estimate of $\tilde{\xi}_{opt}$ can be found as described in Appendix C and in [26].

An overview of the methodology proposed in this study for the estimation of the optimal TLCDI paramters and structural response statistics is illustrated in the flow chart in Fig. 6.

4. Investigation on the optimal design parameters

The main advantage of the proposed approach lies in the straightforward evaluation of the optimal design paramenters. In order to show the accuracy of this proposed simplified approach, a comparison with the optimal values obtained through a numerical iterative procedure is here performed. To this aim, a reference set of system parameters has been selected, and in turn each one has been varied in a wide range of values. Specifically, the reference set of parameters used is: $\omega_s = 4\pi/3$, $\alpha = 0.9$, $\mu_l = 0.04$, $\delta = 0.01$, $\beta = 0.3$, $\zeta_s = 0.01$ and $G_0 = 0.002$ [16, 17]. In this respect, a genetic algorithm (GA procedure) [35] has been used to find those values of $\nu_{l,opt}$, $\nu_{2,opt}$, $\zeta_{2,opt}$ and ξ_{opt} that minimize the displacement variance of the complete nonlinear system in Eq. 2 adopting

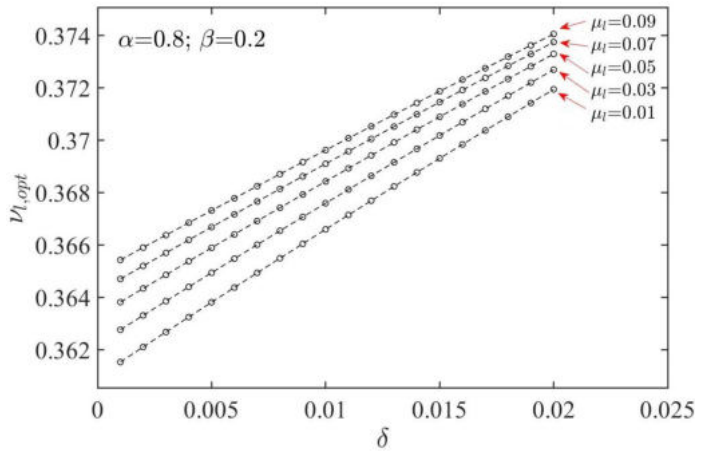

(a)

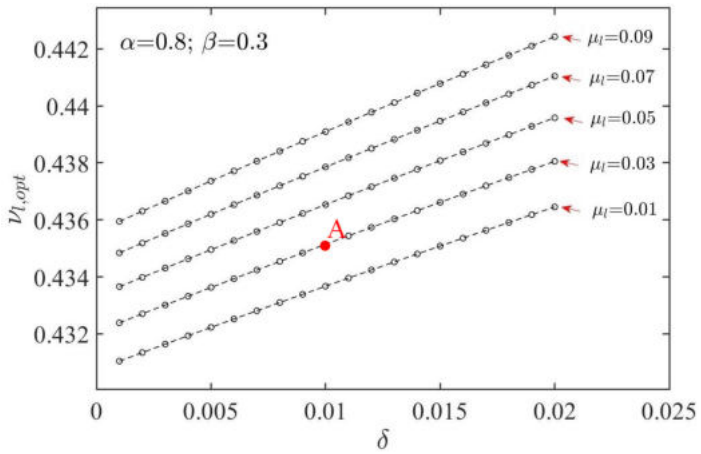

(b)

Figure 5: Optimal design charts in terms of $\nu_{l,opt}$ for several values of μ_l: (a) $\beta = 0.2$ and $\alpha = 0.8$; (b) $\beta = 0.3$ and $\alpha = 0.8$.

the SLT. In order to implement this numerical minimization algorithm, some constraints for the sought TLCDI tuning variables have been applied in terms of lower bound and upper bound vectors, $\mathbf{LB} = [\nu_{2,min}; \zeta_{2,min}; \nu_{l,min}; \xi_{min}]$ and $\mathbf{UB} = [\nu_{2,max}; \zeta_{2,max}; \nu_{l,max}; \xi_{max}]$. Specifically, $\mathbf{LB} = [0.01;0.01;0.1495;1]$ and $\mathbf{UB} = [3;1;0.4728;300]$ have been imposed, respectively, where $\nu_{l,min}$ and $\nu_{l,max}$ have been set by assuming reasonable values of the total liquid length L (a range between L_{min}=5m and L_{max}=50m). Boundary values of the head loss coefficient have been set on the basis of the prediction formula experimetally constructed by [23] to design conventional TLCDs with different area ratios of orifices and considering an upper limit of ζ_l=1 [26].

Note that, in this way, for each iteration of the GA optimization algorithm, an optimum value of ξ_{opt} is found and the iterative SLT must be applied to evaluate the equivalent linear damping ratio ζ_l. Therefore, in this case, a rather elaborate numerical procedure must be implemented.

The optimal design parameters $\tilde{\nu}_{l,opt}$, $\tilde{\nu}_{2,opt}$, $\tilde{\zeta}_{2,opt}$ and $\tilde{\xi}_{opt}$ determined through

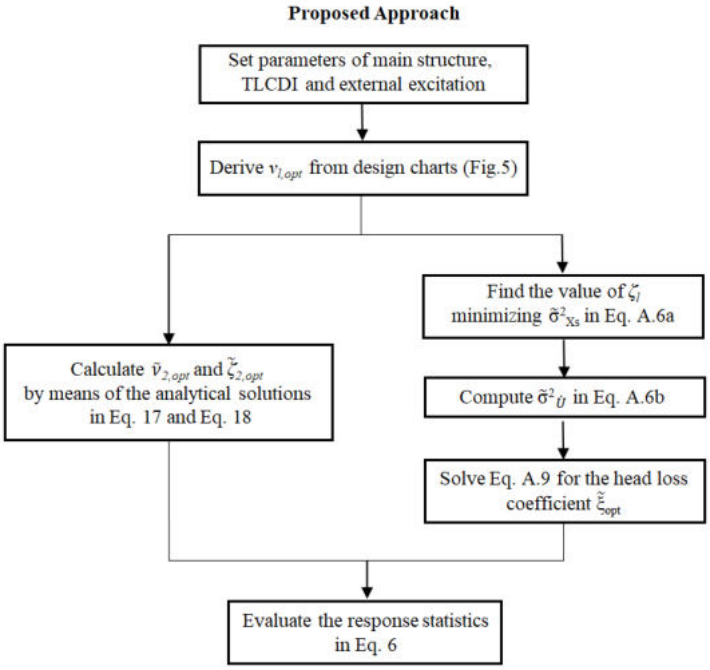

Figure 6: Flow chart of the proposed approximate approach.

the proposed direct approach have been used to compute the displacement variance $\sigma^2_{X_s}$ of the system as in Eq. 6. With reference to the previously defined structural system, the optimal parameters obtained by the proposed approach are listed in Table 1. Results have then been compared with the values obtained by the aforementioned complete numerical GA procedure.

Table 1: Optimal TLCDI design parameters obtained by the proposed approach. Chosen reference set of parameters: $\alpha = 0.9$, $\mu_l = 0.04$, $\beta = 0.3$, $\delta = 0.01$, $G_0 = 0.002$.

		$\tilde{\nu}_{l,opt}$	$\tilde{\nu}_{2,opt}$	$\tilde{\zeta}_{2,opt}$	$\tilde{\xi}_{opt}$
α	0.6	0.4439	2.0416	0.6794	240.42
	0.7	0.4408	2.0327	0.672	219.85
	0.8	0.4372	2.0222	0.6633	205.96
	0.9	0.4331	2.0101	0.6533	196.57
μ_l	0.02	0.4364	2.6086	0.8255	176.24
	0.03	0.4347	2.2532	0.7226	187.08
	0.04	0.4331	2.0101	0.6533	196.57
	0.05	0.4315	1.8302	0.6029	204.99
δ	0.01	0.4331	2.0101	0.6533	196.57
	0.02	0.4363	1.8432	0.6137	192.43
	0.03	0.4393	1.7134	0.5842	188.59
	0.04	0.4422	1.6086	0.5613	185.02
β	0.25	0.3997	1.8985	0.558	245.93
	0.30	0.4331	2.0101	0.6533	196.57
	0.35	0.4642	2.1043	0.7463	160.19
	0.40	0.4728	2.1849	0.8398	151.44

Fig. 7 shows the results in terms of the normalized displacement variance of the SDOF-TLCDI equipped structure $\varepsilon_{X_s} = \sigma^2_{X_s}/\sigma^2_{X_0}$, where $\sigma^2_{X_0}$ is the displacement variance of the system without TLCDI. Note that this parameter may represent also a performance control index for the SDOF-TLCDI controlled structure, since lower values of ε_{X_s} indicate higher control efficacy of the TLCDI.

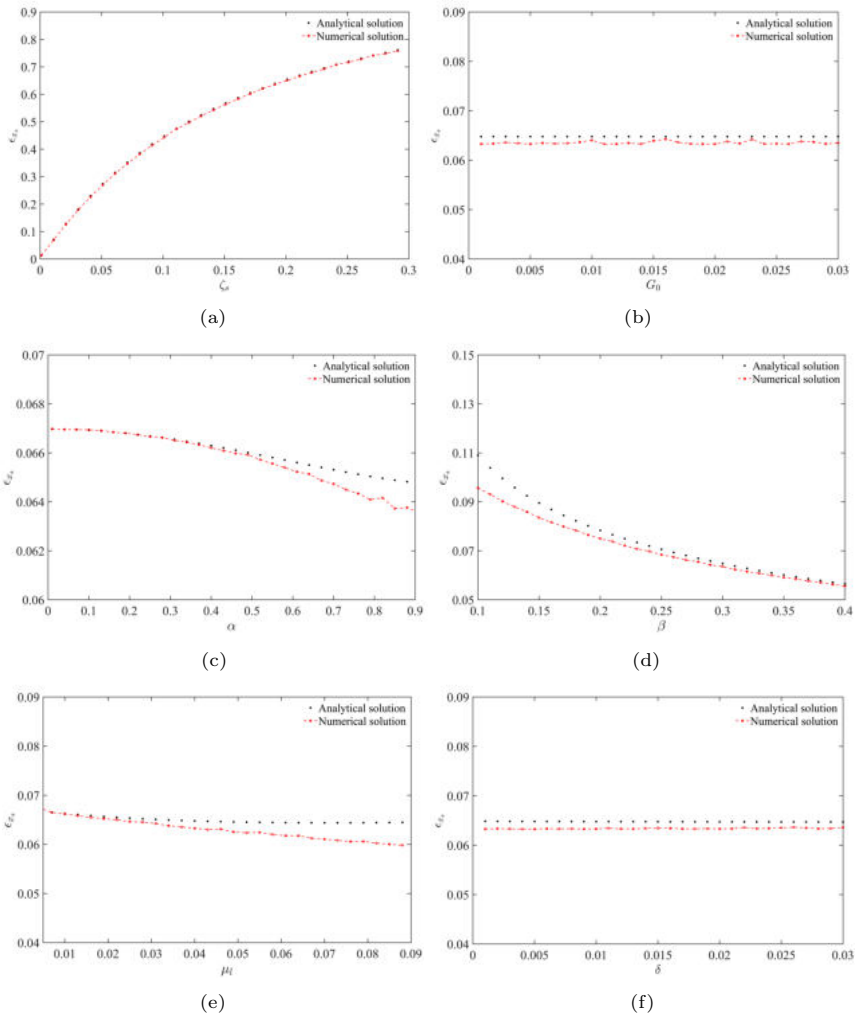

Figure 7: Main system normalized displacement variance: comparison between the numerical GA procedure (dot dashed red line) and the proposed formulation (balck dots) for different parameters.

Specifically, in Fig. 7 the effects of the variation of the structural damping ratio ζ_s, the input intensity G_0, the length ratio α, the inertance ratio β and the mass ratios μ_l and δ on the proposed formulation are shown. The performed parametric analyses show that the response variances computed by the proposed approximated formulation clearly follow those obtained through the GA procedure in the parameters range of practical interest, with differences lower than 10 %, thus assessing the validity of the proposed direct approach.

Clearly, the above described procedure has been derived considering a white noise base excitation. Therefore, further analysis are performed to show the reliability of the proposed approach in case of more generic broad-band earthquake excitation. To this aim, the widely used Clough-Penzien power spectrum can be adopted as a more realistic model of earthquake ground accelerations. This process is characterized by the following one-sided PSD [36, 37]

$$G_{\ddot{X}_g}(\omega) = G_0 \frac{{\omega_g}^4 + 4{\zeta_g}^2{\omega_g}^2\omega^2}{({\omega_g}^2 - \omega^2)^2 + 4{\zeta_g}^2{\omega_g}^2\omega^2} \frac{\omega^4}{({\omega_f}^2 - \omega^2)^2 + 4{\zeta_f}^2{\omega_f}^2\omega^2} \tag{23}$$

where G_0 is the constant white noise PSD, whose value is related to the bedrock peak ground acceleration, while $(\omega_g, \zeta_g, \omega_f, \zeta_f)$ are filter parameters whose values depend on the different soil conditions [38]. Next, taking into account Eq. 6, the corresponding displacement variance $\sigma^2_{X_s}$ can be given as

$$\sigma^2_{X_s} = \int_0^\infty |H_{X_s}(\omega)|^2 G_{\ddot{X}_g}(\omega)\, d\omega \tag{24}$$

where $H_{X_s}(\omega)$ is given in Eq. A.2 in Appendix A.

In this manner, again a numerical optimization employing the GA procedure on Eq. 24 can be used to find the optimal values of the design parameters ($\nu_{2,opt}$, $\zeta_{2,opt}$) also for this model. Once these optimized parameters are found, the corresponding performance control index ε_{X_s} can be evaluated.

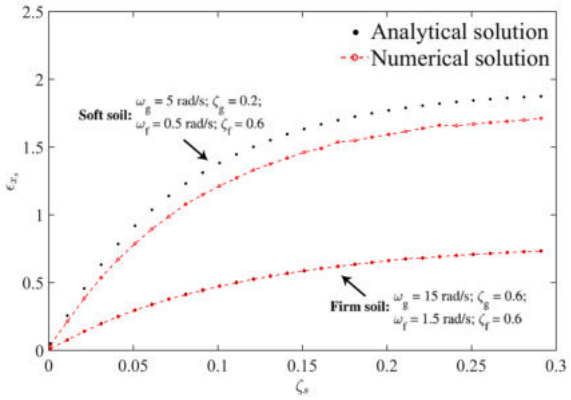

Figure 8: Comparison of the performance control index ε_{X_s} in case of non-white excitation for different values of:the structural damping ratios ζ_s. Analytical based solution (black dots) vis-à-vis numerical complete solution (red dashed-dot line).

In this regard, values of ε_{X_s} computed via the numerical-based procedure vis-à-vis pertinent values obtained using optimal parameters provided by the proposed analytical approach are shown in Fig. 8 for a wide range of the structural damping ratios ζ_s.

As it can be seen in this figure, even assuming a non-white earthquake excitation the performance control index ε_{X_s} obtained using the optimal values found by following the proposed approach (black dots) closely agrees with the one obtained with the numerical solution (red dashed-dot line), also for different soil conditions (firm and soft soil).

Therefore, since so small discrepancies are obtained between the two procedures in terms of control performance parameter ε_{X_s}, and considering the significant reduction in computational effort achieved, the proposed direct approach can effectively be regarded as a powerful and reliable tool to be employed for the evaluation of the optimal design parameters.

5. Analysis of the control performance

To show the reliability of the proposed approach considering also the non-stationary nature of real earthquake ground motions, in this section the control performance of the SDOF system equipped with a TLCDI device is examined by using time-history analyses with selected recorded accelerograms. Specifically, the Imperial Valley (USA, 09/15/1979) (Fig. 9a) and Kobe (Japan, 17/01/1995) (Fig. 9b) recorded earthquakes, taken among the 44 recorded ground motions of the FEMAP695 far-field (FEMAP695) set [39], have been used as base accelerations. Note that these earthquakes records present quite different characteristics. Specifically, the latter has high impulsive content in the first instants of motion, which is known to be detrimental for the efficiency of the control system.

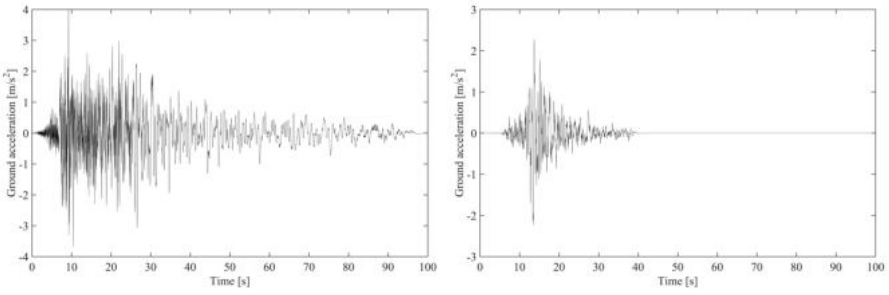

(a) (b)

Figure 9: Earthquake records: (a) Imperial Valley (USA, 09/15/1979); (b) Kobe (Japan, 17/01/1995).

To properly account for the nonlinear features of the system with TLCDI device, direct numerical solution of the pertinent equation of motions of the complete systems (Eqs. 1) has been performed using a 4th order Runge-Kutta algorithm. The seismic response of the uncontrolled system has been compared with the same systems equipped with the proposed TLCDI and traditional TLCD.

The liquid inside the TLCDI and TLCD container is assumed to be water ($\rho = 997 kg/m^3$), assuming a value of the mass ratio μ_l of 4% for both devices and the length ratio α is set to 0.9 [20]. The TLCDI inertance ratio β is assumed to be equal to 0.3 and the value of the mass ratio of the water tank δ is fixed to 1% [20].

Two benchmark structures, denoted as "Structure 1" and "Structure 2", have been considered for the numerical analyses. Structure 1 is characterized by a natural frequency $\omega_{s_1} = 4\pi/3$ and damping ratio $\zeta_s = 0.01$, while Structure 2 by a frequency $\omega_{s_2} = 2\omega_{s_1}$ and the same damping ratio. The TLCDI optimal parameters have been obtained by the proposed simplified approach, while the TLCD optimal parameters by applying the optimization procedure discussed in

[25]. The optimal parameters obtained by means of the the proposed procedure are: $\tilde{\nu}_{l,opt} = 0.4331$, $\tilde{\nu}_{2,opt} = 2.0101$, $\tilde{\zeta}_{2,opt} = 0.6533$ and $\tilde{\xi}_{opt} = 196.57$ for Structure 1, and $\tilde{\nu}_{l,opt} = 0.2364$, $\tilde{\nu}_{2,opt} = 1.9964$, $\tilde{\zeta}_{2,opt} = 0.6902$ and $\tilde{\xi}_{opt} = 266.768$ for Structure 2, respectively.

Figs. 10a- 10b show the displacement responses of both structures, with the proposed TLCDI, the traditional TLCD and without any devices, and subjected to the Imperial Valley earthquake record. As it can be seen, the TLCDI device is particularly effective in reducing the displacement, with a clear reduction of the peak displacement. Moreover, as it can be seen, the difference in frequency between the two structures does not affect the control performance. The time histories of the absolute acceleration responses of the two structural typologies are also presented in Figs. 11a- 11b, respectively. Once again, the best mitigation effect is achieved by the system controlled with the TLCDI. Similar results can be observed for the Kobe earthquake (Fig. 12- 13). Note that, also for this particular case of impulsive ground motion, the use of the TLCDI improves appreciably the performance control of the system.

The peak responses based on the time histories of the responses of the structures shown in Figs. 10- 13, are listed in Table 2 for the Structure 1 and in Table 3 for the Structure 2. As it can be read from Table 3, the best performance of the TLCDI-controlled systems is observed for Structure 2 subjected to the Imperial Valley record, with a reduction of 64% for the structural displacement response and 69% on the peak acceleration. Furthermore, in the worst-case scenario, the peak of displacement of Structure 2 (i.e. 0.1183 m) for the Kobe earthquake can be reduced of 52% when the TLCDI is applied against the reduction of 13% when the TLCD is used. Based on the overall consideration of these results, TLCDI is more effective in reducing the peak responses than the TLCD.

On this base, it can be argued that, although being developed assuming a white noise base excitation, the proposed analytical solution yields optimal design parameters that lead to satisfactory control performances also for real earthquake records.

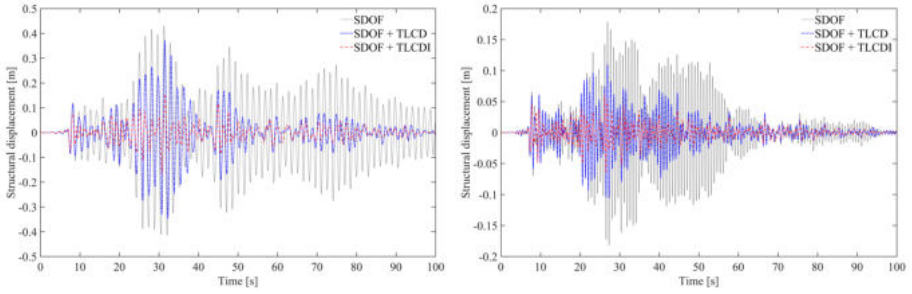

(a) (b)

Figure 10: Response in terms of structural displacements to the Imperial Valley earthquake: (a) Structure 1; (b) Structure 2; SDOF system with TLCDI - red dashed line; SDOF system with TLCD - blue dot-dashed line; uncontrolled SDOF system – black line.

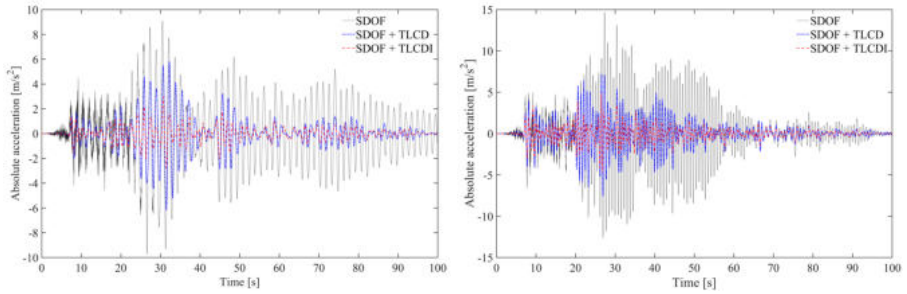

(a) (b)

Figure 11: Response in terms of absolute accelerations to the Imperial Valley earthquake: (a) Structure 1; (b) Structure 2; SDOF system with TLCDI - red dashed line; SDOF system with TLCD - blue dot-dashed line; uncontrolled SDOF system – black line.

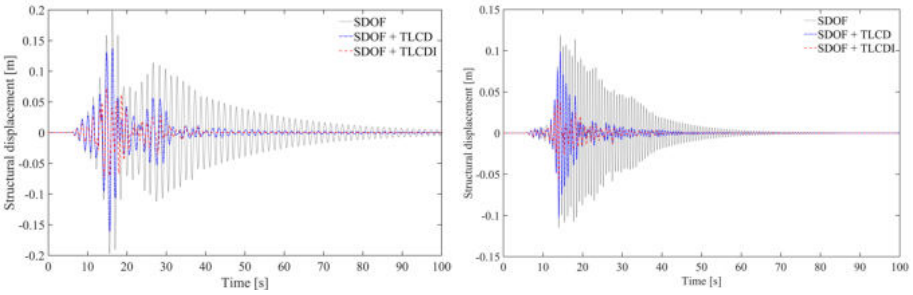

(a) (b)

Figure 12: Response in terms of structural displacements to the Kobe earthquake: (a) Structure 1; (b) Structure 2; SDOF system with TLCDI - red dashed line; SDOF system with TLCD - blue dot-dashed line; uncontrolled SDOF system – black line.

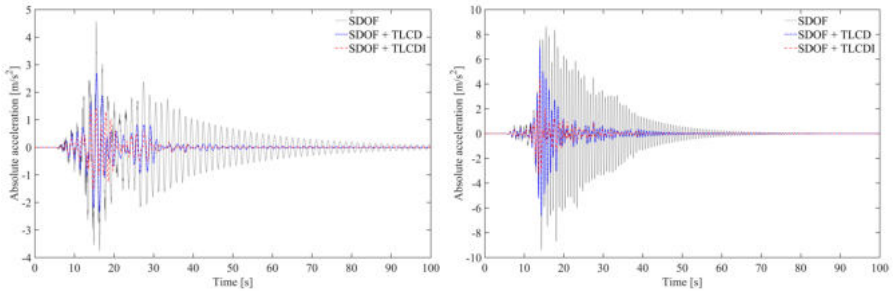

(a) (b)

Figure 13: Response in terms of absolute accelerations to the Kobe earthquake: (a) Structure 1; (b) Structure 2; SDOF system with TLCDI - red dashed line; SDOF system with TLCD - blue dot-dashed line; uncontrolled SDOF system – black line.

Table 2: Maximum values of the responses of the SDOF system (Structure 1) and of the SDOF system coupled with TLCDI.

Excitation: Imperial Valley record		
Case	Max structural displacement $max\|x_s(t)\|$ [m]	Max structural acceleration $max\|a(t)\|[m/s^2]$
SDOF	0.4316	9.7643
SDOF+TLCD	0.3715	6.2035
SDOF+TLCDI	0.1622	2.9517
Excitation: Kobe record		
SDOF	0.1986	4.5919
SDOF+TLCD	0.1613	2.7066
SDOF+TLCDI	0.0744	1.5197

Table 3: Maximum values of the responses of the SDOF system (Structure 2) and of the SDOF system coupled with TLCDI.

Excitation: Imperial Valley record		
Case	Max structural displacement $max\|x_s(t)\|$ [m]	Max structural acceleration $max\|a(t)\|[m/s^2]$
SDOF	0.1820	14.7016
SDOF+TLCD	0.1103	7.5731
SDOF+TLCDI	0.0662	4.8814
Excitation: Kobe record		
SDOF	0.1183	9.4129
SDOF+TLCD	0.1027	6.9973
SDOF+TLCDI	0.0562	4.3876

6. Concluding remarks

In this paper, the optimization and pertinent control performances of the TLCDI passive control device, recently introduced in the literature, have been investigated for reducing the structural response of a SDOF structure under seismic base excitations. The additional inerter mechanism in the TLCDI greatly enhances the efficiency of the classical TLCD, making the TLCDI an appealing lightweight control device with outperforming control performances compared to conventional TLCDs.

An optimal design of the TLCDI through closed form solutions and useful design charts has been proposed by considering a Gaussian white noise model of the base excitation and minimizing the structural displacement variance of the system, resorting to the tool of the Statistical Linearization Technique.

In order to prove the reliability of the proposed approach, comparison with a rather elaborate numerical optimization procedure has been performed for both white noise and broad-band earthquake excitation to take into account additional features of the seismic excitation.

Results show a satisfactory agreement in terms of control performances between the proposed analytical approach and the numerical one. Note that the use of analytical expressions and ready-to-use design charts provided by the

proposed straightforward procedure leads to a significant reduction in computational effort.

Moreover, to show the influence of the non-stationary nature of real earthquakes, the seismic response of two types of SDOF systems, characterized by different frequencies and equipped with a TLCDI device, has been examined under different recorded ground motion accelerations. Comparisons with the uncontrolled systems and the systems equipped with the classical TLCD have been carried out. Both TLCD and TLCDI device can efficiently control the earthquake-induced displacement and absolute acceleration responses of the primary SDOF structure. However, results indicate that the TLCDI presents significantly enhanced control performances with respect to the TLCD in all the cases. Specifically, time history analyses show that the TLCDI device, designed by employing the proposed approach, can lead to a 64% reduction on the peak displacement and 69% on the peak acceleration, with respect to the case of the structure without TLCDI.

Overall, results of the performed analyses have clearly assessed the reliability of the proposed optimization procedure even for non-stationary broad-band base excitations, proving that the TLCDI can be regarded as a lightweight-based control means to achieve an improved control performance.

Acknowledgements

A. Di Matteo, C. Masnata, and A. Pirrotta gratefully acknowledge the support received from the Italian Ministry of University and Research, through the PRIN 2017 funding scheme (project 2017J4EAYB 002 - Multiscale Innovative Materials and Structures "MIMS"). A. Di Matteo gratefully acknowledge the financial support of the project PON R&I 2014-2020-AIM (Attraction and International Mobility), project AIM1845825-1.

Appendix A

In this appendix the displacement transfer functions of the equivalent linear system in Eq. 3 are presented. In this respect, making the Fourier transform of Eq. 3, yields

$$\begin{aligned}
&X_s(\omega)\left[-(1+\mu_t+\delta)\omega^2+2i\omega\omega_s\zeta_s+{\omega_s}^2\right]-(\mu_t+\delta)\omega^2Y(\omega)-\alpha\mu_lU(\omega)=\\
&=-(1+\mu_t)\ddot{X}_g(\omega)\\
&Y(\omega)\left[-(\mu_t+\delta)\omega^2+2i\omega\omega_2\zeta_2\mu_t+\mu_t{\omega_2}^2\right]-\omega^2\left(\mu_t+\delta\right)X_s(\omega)-\alpha\mu_l\omega^2U(\omega)=\\
&=-\mu_t\ddot{X}_g(\omega)\\
&U(\omega)\left[-\omega^2+2i\omega\omega_l\zeta_l+{\omega_l}^2\right]-\omega^2\alpha X_s(\omega)-\omega^2\alpha Y(\omega)=-\alpha\ddot{X}_g(\omega)
\end{aligned} \tag{A.1}$$

Therefore, the main structure displacement transfer function ($H_{X_s}(\omega)=$ $=X_s(\omega)/\ddot{X}_g(\omega)$) can be written as

$$H_{X_s}(\omega)=\frac{b(\omega)c(\omega)(1+\mu_t)+\left[b(\omega)\alpha^2\mu_l+c(\omega)\mu_t(\mu_t+\delta)\right]\omega^2+\alpha^2\mu_l(-1+\mu_t+\delta)\omega^4}{-a(\omega)b(\omega)c(\omega)+\left[(a(\omega)+b(\omega))^2\alpha^2\mu_l+c(\omega)(\mu_t+\delta)^2\right]\omega^4+2\alpha^2\mu_l(\mu_t+\delta)\omega^6} \tag{A.2}$$

while the container displacement and liquid column transfer functions ($H_Y(\omega)=$ $=Y(\omega)/\ddot{X}_g(\omega)$ and $H_U(\omega)=U(\omega)/\ddot{X}_g(\omega)$) respectively are

$$\begin{aligned}
H_Y(\omega)&=H_{X_s}(\omega)\frac{a(\omega)c(\omega)\mu_t+\left[a(\omega)\alpha^2\mu_l+c(\omega)(1+\mu_t)(\mu_t+\delta)\right]\omega^2+\alpha^2\mu_l(1+\mu_t+\delta)\omega^4}{b(\omega)c(\omega)(1+\mu_t)+\left[b(\omega)\alpha^2\mu_l+c(\omega)\mu_t(\mu_t+\delta)^2\right]\omega^2+2\alpha^2\mu_l(-1+\mu_t+\delta)\omega^4}\\
H_U(\omega)&=\frac{\alpha}{c(\omega)}\left[-1+\omega^2H_{X_s}(\omega)+\omega^2H_Y(\omega)\right]
\end{aligned} \tag{A.3}$$

with

$$a(\omega)=-(1+\mu_t+\delta)\omega^2+2i\omega\omega_s\zeta_s+{\omega_s}^2 \tag{A.4a}$$

$$b(\omega)=-(\mu_t+\delta)\omega^2+2i\omega\omega_2\zeta_2\mu_t+\mu_t{\omega_2}^2 \tag{A.4b}$$

$$c(\omega)=-\omega^2+2i\omega\,\zeta_l\omega_l+{\omega_l}^2 \tag{A.4c}$$

These parameters can be directly used to evaluate the statistics of the equivalent linear system in Eq. 3, necessary for the iterative SLT. It is worth noting that once the closed-form expression for these transfer functions have been computed, the response statistics in terms of container displacement and liquid displacement can be immediately determined numerically solving the following equations:

$$\sigma_Y^2=\int_0^\infty|H_Y(\omega)|^2G_0\,d\omega, \tag{A.5a}$$

$$\sigma_U^2=\int_0^\infty|H_U(\omega)|^2G_0\,d\omega \tag{A.5b}$$

Appendix B

In order to propose an effective and direct tool for pre-designing TLCDI devices, additional charts are provided in this Appendix. In paricular, some design charts, reporting optimal values directly in terms of $\tilde{\nu}_{l,opt}$, are depicted in Fig. .14, based on Eq. 17 and Eq. 18. The design charts, have been evaluated for α=0.6 and α=0.9 for different values of mass ratio μ_l and inertance ratio β.

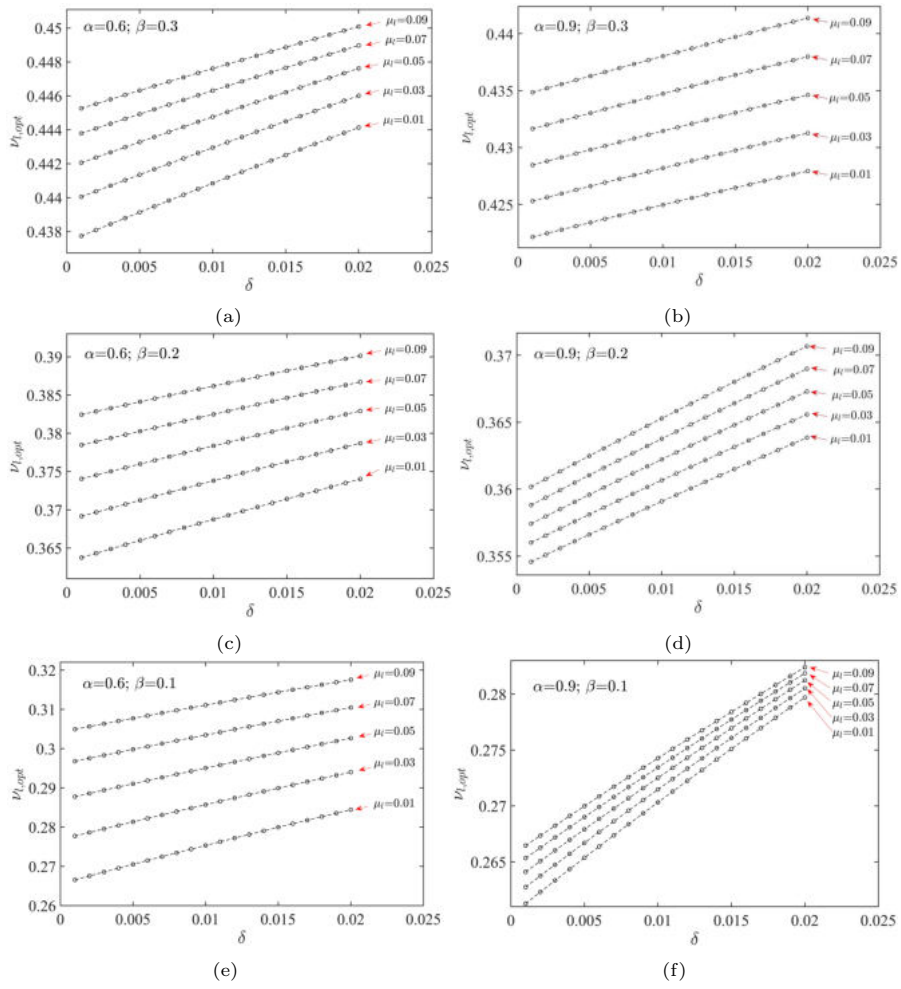

Figure .14: Optimal design charts in terms of $\nu_{l,opt}$ for several values of μ_l: (a) $\beta = 0.3$ and $\alpha = 0.6$; (b) $\beta = 0.3$ and $\alpha = 0.9$; (c) $\beta = 0.2$ and $\alpha = 0.6$; (d) $\beta = 0.2$ and $\alpha = 0.9$;(e) $\beta = 0.1$ and $\alpha = 0.6$; (f) $\beta = 0.1$ and $\alpha = 0.9$.

Appendix C

As far as the estimation of the head loss coefficient is concerned, according to the anlysis developed in [26] for TLCD-controlled SDOF structures, an indicative value can be obtained by firstly considering the main system displacement and the fluid velocity variances of the SDOF structure with classical TLCD, which can be expressed as:

$$\tilde{\sigma}^2_{X_s} = \frac{\pi G_0}{4\tilde{z}_{X_s}\omega_s^3}, \tag{A.6a}$$

$$\tilde{\sigma}^2_{\dot{U}} = \frac{\pi G_0}{4\tilde{z}_{\dot{U}}\omega_l} \tag{A.6b}$$

where $\tilde{z}_{X_s}$ and $\tilde{z}_{\dot{U}}$ depend on both ν_l and ζ_l and have the following expressions

$$\tilde{z}_{X_s} = \frac{N_{Z_{X_s}}}{D_{Z_{X_s}}}, \tag{A.7a}$$

$$\tilde{z}_{\dot{U}} = \frac{N_{Z_{X_s}}}{D_{Z_{\dot{U}}}} \tag{A.7b}$$

The numerator $N_{Z_{X_s}}$ and denominator $D_{Z_{X_s}}$ of $\tilde{z}_{X_s}$ and $D_{Z_{\dot{U}}}$ of $\tilde{z}_{\dot{U}}$ are given by:

$$\begin{aligned}
&N_{Z_{X_s}} = \zeta_s\zeta_l + \zeta_2^2\left(4\zeta_s^2 + \alpha^2\mu_l\right)\nu_l + 2\zeta_s\zeta_l\left[2\zeta_s^2 + \alpha^2\mu_l + (2\zeta_l^2 - 1)(1+\mu_l)\right]{\nu_l}^2 + \\
&+\zeta_s^2\left[\alpha^2\mu_l + 4\zeta_l^2(1+\mu_l)\right]{\nu_l}^3 + \zeta_s\zeta_l(1+\mu_l)^2{\nu_l}^4 \\
&D_{Z_{X_s}} = \zeta_l\left(1+\mu_l-\alpha^2\mu_l\right)^2 + \zeta_s\left[\alpha^4\mu_l^2 + 4\zeta_l^2(1+\mu_l)^2\right]\nu_l + \zeta_l(1+\mu_l)^2[4\zeta_s^2 + \\
&+3\alpha^2\mu_l + \left(4\zeta_l^2 - 2\right)(1+\mu_l)]{\nu_l}^2 + \zeta_s(1+\mu_l)^2\left[\alpha^2\mu_l + 4\zeta_l^2(1+\mu_l)\right]{\nu_l}^3 + \zeta_l(1+\mu_l)^4{\nu_l}^4 \\
&D_{Z_{\dot{U}}} = \alpha^2\left[\zeta_s + \zeta_l\left(1+\mu_l+4\zeta_s^2\right)\nu_l + 4\zeta_s^3{\nu_l}^2\right]
\end{aligned} \tag{A.8}$$

By minimizing Eq. A.6a considering the input structural parameters and the optimal value $\nu_{l,opt}$ obtained by means of the proposed procedure, the optimal value of the equivalent damping ratio ζ_l can be obtained. Next, by setting this value in Eq. A.6b, the fluid velocity variance can be computed so that the value of $\tilde{\xi}_{opt}$ can be evaluated from Eq. 5 as

$$\tilde{\xi}_{opt} = 2L\zeta_l\nu_l\omega_s\sqrt{\frac{\pi}{2\tilde{\sigma}_{\dot{U}}}} \tag{A.9}$$

It is worth noting that, if a classical procedure is used to define the equivalent damping ratio ζ_l, a time-consuming iterative scheme has to be set up. Conversely, following the herein proposed approach, the evaluation of the optimal values can be obtained by means of a numerical minimization of a smooth function (Eq. A.6a), without any iteration, thus resulting in a significant reduction in computational effort.

References

[1] Frahm, H., Device for damping vibrations of bodies (1909).

[2] Den Hartog, J. P., Mechanical Vibrations, New York, NY: McGraw-Hil, 1956.

[3] Banerji, P., Murudi, M., Shah, A. H., Popplewell, N., Tuned liquid dampers for controlling earthquake response of structures, Earthquake Engineering & Structural Dynamics 29 (5) (2000) 587–602. doi:https://doi.org/10.1002/(SICI)1096-9845(200005)29:5<587::AID-EQE926>3.0.CO;2-I.

[4] Pandey, D. K., Sharma, M. K., Mishra, S. K., A compliant tuned liquid damper for controlling seismic vibration of short period structures, Mechanical Systems and Signal Processing 132 (2019) 405–428. doi:https://doi.org/10.1016/j.ymssp.2019.07.002.
URL https://www.sciencedirect.com/science/article/pii/S0888327019304315

[5] Pabarja, A., Vafaei, M., Alih, S. C., Yatim, M. Y. M., Osman, S. A., Experimental study on the efficiency of tuned liquid dampers for vibration mitigation of a vertically irregular structure, Mechanical Systems and Signal Processing 114 (2019) 84–105. doi:10.1016/j.ymssp.2018.05.008.

[6] Sakai, F., Takeda, S., Tamaki, T., Tuned liquid column damper- new type device for suppression of building vibrations, in: Proceedings of the international conference on highrise buildings, Nanjing, China, 1989, pp. 926–931.

[7] Hochrainer, M.J., Ziegler, F., Control of tall building vibrations by sealed tuned liquid column damper, Structural Control and Health Monitoring 13 (6) (2006) 980–1002.

[8] M. Smith, Synthesis of mechanical networks: the inerter, IEEE Transactions on Automatic Control 47 (10) (2002) 1648–1662.
URL https://doi.org/10.1109/TAC.2002.803532

[9] Papageorgiou, C., Smith, M. C., Laboratory experimental testing of inerters, in: Proceedings of the 44th IEEE Conference on Decision and Control, 2005, pp. 3351–3356. doi:10.1109/CDC.2005.1582679.

[10] Ikago, K., Saito, K., Inoue, N., Seismic control of single-degree-of-freedom structure using tuned viscous mass damper, Earthquake Engineering & Structural Dynamics 41 (3) (2012) 453–474. doi:https://doi.org/10.1002/eqe.1138.

[11] Garrido, H., Curadelli, O., Ambrosini, D., Improvement of tuned mass damper by using rotational inertia through tuned viscous mass damper, Eng. Struct. 56 (2013) 2149–2153.

[12] Smith, M., The Inerter: A Retrospective, Annual Review of Control, Robotics, and Autonomous Systems 3 (2020) 361–391. doi:10.1146/annurev-control-053018-023917.

[13] Giaralis, A., An Inerter-Based Dynamic Vibration Absorber With Concurrently Enhanced Energy Harvesting and Motion Control Performances Under Broadband Stochastic Excitation Via Inertance Amplification, ASCE-ASME J Risk and Uncert in Engrg Sys Part B Mech Engrgdoi:10.1115/1.4049213.

[14] Takewaki, I., Murakami, S., Yoshitomi, S., Tsuji, M., Fundamental mechanism of earthquake response reduction in building structures with inertial dampers, Structural Control and Health Monitoring 19 (6) (2012) 590–608. doi:https://doi.org/10.1002/stc.457.

[15] Marian, L., Giaralis, A., Probabilistic Engineering Mechanics 156–164.

[16] De Domenico, D., Ricciardi, G., An enhanced base isolation system equipped with optimal tuned mass damper inerter (TMDI), Earthquake Engineering & Structural Dynamics 47 (5) (2018) 1169–1192.
URL https://doi.org/10.1002/eqe.3011

[17] Di Matteo, A., Masnata, C., Pirrotta, A., Simplified analytical solution for the optimal design of Tuned Mass Damper Inerter for base isolated structures, Mechanical Systems and Signal Processing 134 (2019) 106337.
URL http://www.sciencedirect.com/science/article/pii/S0888327019305588

[18] Masnata, C., Di Matteo, A., Adam, C., Pirrotta, A., Smart structures through nontraditional design of Tuned Mass Damper Inerter for higher control of base isolated systems, Mechanics Research Communications 105 (2020) 103513.
URL 10.1016/j.mechrescom.2020.103513

[19] Z. Zhao, R. Zhang, Y. Jiang, C. Pan, A tuned liquid inerter system for vibration control, International Journal of Mechanical Sciences 164 (2019) 105171. doi:https://doi.org/10.1016/j.ijmecsci.2019.105171.
URL http://www.sciencedirect.com/science/article/pii/S0020740319320715

[20] Wang, Q., Tiwari, N. D., Qiao, H., Wang, Q., Inerter-based tuned liquid column damper for seismic vibration control of a single-degree-of-freedom structure, International Journal of Mechanical Sciences 184 (2020) 105840. doi:10.1016/j.ijmecsci.2020.105840.

[21] Wang, Q., Qiao, H., De Domenico, D., Zhu, Z., Tang, Y., Seismic response control of adjacent high-rise buildings linked by the Tuned Liquid Column Damper-Inerter (TLCDI), Engineering Structures 223 (2020) 111169. doi:10.1016/j.engstruct.2020.111169.

[22] Hitchcock, P.A., Kwok, K.C.S., Watkins, R.D., Samali, B., Characteristics of liquid column vibration absorbers (LCVA)—I, Engineering Structures 19 (2) (1997) 126–134. doi:https://doi.org/10.1016/S0141-0296(96)00042-9.
URL https://www.sciencedirect.com/science/article/pii/S0141029696000429

[23] Wu, J.-C., Shih, M.-H., Lin, Y-Y., Shen, Y.-C., Design guidelines for tuned liquid column damper for structures responding to wind, Engineering Structures 27 (13) (2005) 1893–1905. doi:https://doi.org/10.1016/j.engstruct.2005.05.009.
URL https://www.sciencedirect.com/science/article/pii/S0141029605002002

[24] Wu, J.-C., Chang, C.-H., Lin Y.-Y., Optimal designs for non-uniform tuned liquid column dampers in horizontal motion, Journal of Sound and Vibration 326 (1) (2009) 104–122. doi:https://doi.org/10.1016/j.jsv.2009.04.027.
URL https://www.sciencedirect.com/science/article/pii/S0022460X09003526

[25] Di Matteo, A., Lo Iacono, F., Navarra, G., Pirrotta, A., Direct evaluation of the equivalent linear damping for TLCD systems in random vibration for pre-design purposes, International Journal of Non-Linear Mechanics 63 (2014) 19–30.
URL http://www.sciencedirect.com/science/article/pii/S0020746214000614

[26] Di Matteo, A., Lo Iacono, F., Navarra, G., Pirrotta, A., Optimal tuning of tuned liquid column damper systems in random vibration by means of an approximate formulation, Meccanica 50 (3) (2015) 795–808.
URL https://doi.org/10.1007/s11012-014-0051-6

[27] Di Matteo, A., Furtmüller, T., Adam, C., Pirrotta, A., Optimal design of tuned liquid column dampers for seismic response control of base-isolated structures, Acta Mechanica 229 (2018) 437–454. doi:10.1007/s00707-017-1980-7.

[28] Chang, C.C., Hsu, C.T., Control performance of liquid column vibration absorbers, Engineering Structures 20 (7) (1998) 580–586. doi:https://doi.org/10.1016/S0141-0296(97)00062-X.
URL https://www.sciencedirect.com/science/article/pii/S014102969700062X

[29] Spanos, P. D., Stochastic Linearization In Structural Dynamics, Applied Mechanics Reviews 34 (1) (1981) 1–8.

[30] Roberts, J.B., Spanos, P.D., Random Vibration and Statistical Linearization, Chichester, 1990.

[31] Di Matteo, A., Lo Iacono, F., Navarra, G., Pirrotta, A., Experimental validation of a direct pre-design formula for TLCD, Engineering Structures 75 (2014) 528–538.
URL https://doi.org/10.1016/j.engstruct.2014.05.045

[32] Di Paola, M., Elishakoff, I., Non-stationary response of linear systems under stochastic Gaussian and non-Gaussian excitation: a brief overview of recent results, Chaos, Solitons & Fractals 7 (7) (1996) 961–971. doi:https://doi.org/10.1016/0960-0779(95)00090-9.
URL https://www.sciencedirect.com/science/article/pii/0960077995000909

[33] Tait, M., Modelling and preliminary design of a structure-TLD system, Engineering Structures 30 (2008) 2644–2655. doi:10.1016/j.engstruct.2008.02.017.

[34] Bekdas, G., Nigdeli, S., Mass ratio factor for optimum tuned mass damper strategies, International Journal of Mechanical Sciences 71 (2013) 68–84. doi:10.1016/j.ijmecsci.2013.03.014.

[35] Goldberg, D. E., Holland, J. H., Genetic Algorithms and Machine Learning, Machine Learning 3 (1988) 95–99. doi:https://doi.org/10.1023/A:1022602019183.

[36] De Domenico, D., Ricciardi, G., Optimal design and seismic performance of tuned mass damper inerter (TMDI) for structures with nonlinear base isolation systems, Earthq. Eng. Struct. Dyn. 47 (2018) 2539–2560.

[37] Clough, R.W., Penzien, J., Dynamics of Structures, Computers and Structures Inc., Berkeley, 2003.

[38] Der Kiureghian, A., Neuenhofer, A., Response spectrum method for multi-support seismic excitations, Earthq. Eng. Struct. Dyn. 21 (1992) 713–740.

[39] FEMA P-695 (Federal Emergency Management Agency), Quantification of Building Seismic Performance Factors, Tech. rep., Federal Emergency Agency, Washington DC (2009).